Supplementary Data

Supplementary Materials and Methods

Construction of human peroxiredoxin 4 transgenic mice and endogenous mouse peroxiredoxin 4 knockout mice (mPRDX4$^{-/y}$)

The primers for human peroxiredoxin 4 (*hPRDX4*) were designed based on a published sequence (Genebank accession no. NM_006406). *hPRDX4* cDNA was amplified by reverse transcription–polymerase chain reaction and cloned into the pGEM-T easy vector system (Invitrogen, Life Technologies Japan Ltd.), as previously described (Supplementary Fig. S1A) (1, 3, 6). The *Not*I fragment containing *hPRDX4* cDNA was inserted into the *Not*I site of pcDNA3 (5.4 kb; Invitrogen, Life Technologies Japan Ltd.), and a bovine growth hormone polyadenylation (BGHPA) sequence was inserted into the tail of the transgene to stabilize expression. The entire nucleic acid sequence, containing a 0.6-kb cytomegalovirus (CMV) enhancer/promoter, the 0.8-kb *hPRDX4* cDNA, and the 0.2-kb BGHPA sequence, was purified by restriction enzyme digestion with *Bgl*II and *Sma*I, and was microinjected into the male pronuclei of one-cell C57BL/6 mouse embryos using standard transgenic (Tg) techniques to generate Tg mice. The CMV enhancer/promoter shows extensive cross talk with other promoters because it contains many transcription factor-binding sites, including two activator protein 1 (AP1), four nuclear factor-kappa B, and five cAMP response element binding protein (CREB)-binding sites (1, 3). Thus, this CMV enhancer/promoter can be stimulated by oxidative stress and/or inflammation. However, as it is not a tissue-specific promoter, the protein expression of the *hPRDX4* transgene

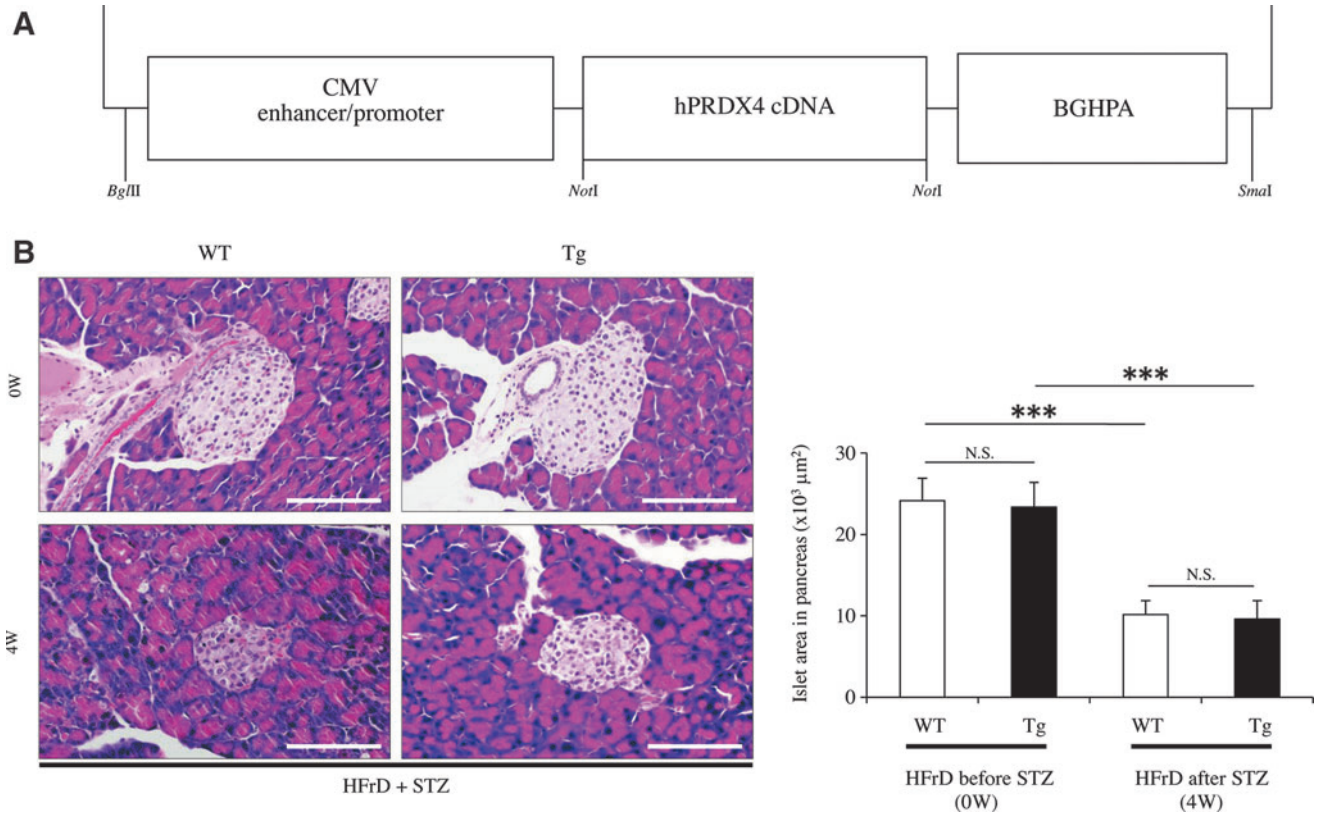

SUPPLEMENTARY FIG. S1. Design of the human peroxiredoxin 4 (hPRDX4) transgene, and comparison of pancreatic islet area between wild-type (WT) and transgenic (Tg) mice following induction of the nongenetic mouse model. (A) *hPRDX4* cDNA (0.8 kb) was driven by a cytomegalovirus (CMV) enhancer/promoter (0.6 kb). A bovine growth hormone (BGH) polyadenylation (polyA) sequence (0.2 kb) was inserted into the transgene to stabilize expression. The construct was purified from 5.4-kb pcDNA3 sequence by restriction digestion with *Bgl*II and *Sma*I. **(B)** There was no difference in the pancreatic islet area between control WT ($24.1 \pm 2.8 \times 10^3$ μm^2) and Tg mice ($23.4 \pm 3.0 \times 10^3$ μm^2) before streptozotocin (STZ) injection ($n = 10$ mice per group). The pancreatic islet area significantly decreased in Tg and WT mice at 4 weeks high-fructose diet (HFrD) feeding and STZ injection (HFrD + STZ), but was not significantly different between the two genotypes (WT $10.2 \pm 1.7 \times 10^3$ μm^2 *vs.* Tg $9.6 \pm 2.3 \times 10^3$ μm^2). Values are means ± standard error (SE). Original magnification: ×200. Scale bar = 80 μm. ***$p < 0.0001$.

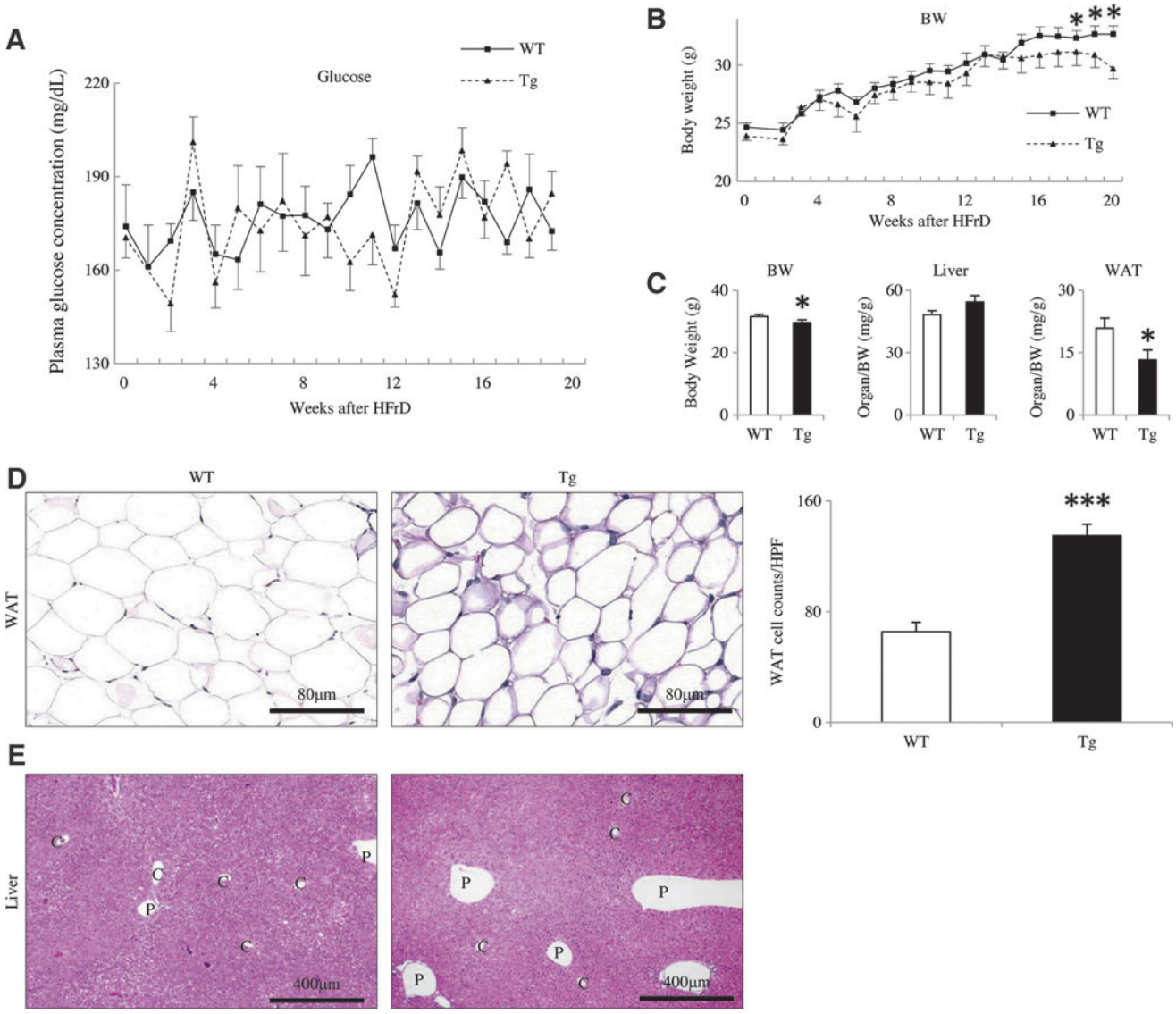

SUPPLEMENTARY FIG. S2. Comparison of metabolic and tissue characteristics between WT and Tg mice fed the HFrD without STZ injection. (A) Blood glucose concentrations did not increase significantly in either WT or Tg mice after being fed the HFrD for 20 weeks, and no significant differences were found between the two groups (HFrD alone, $n=8$ mice per group). **(B)** The increase in body weight (BW) at 18–20 weeks was significantly slower and smaller in HFrD-fed Tg mice than in HFrD-fed WT mice (HFrD alone, $n=8$ mice per group). **(C)** The BW and white adipose tissue (WAT)/BW ratio was significantly lower in HFrD-fed Tg mice than in HFrD-fed WT mice after 20 weeks of HFrD feeding (HFrD alone, $n=8$ mice per group). **(D)** The number of adipocytes in WAT was significantly greater in HFrD-fed Tg mice than in HFrD-fed WT mice (HFrD alone, $n=8$ mice per group). Original magnification: ×200, scale bar = 80 μm. **(E)** Histological examination of the liver revealed no remarkable changes in HFrD-fed WT or HFrD-fed Tg mice, nor was there any clear evidence of NAFLD in either genotype (HFrD alone, $n=8$ mice per group). C, central vein; P, portal vein. Original magnification: ×40, scale bar = 400 μm. Values are means ± SE. *$p<0.05$. ***$p<0.0001$.

will be affected according to its site of integration into the mouse genome. C57BL/6 mice (Charles River Laboratories) were used as the control wild-type (WT) mice in this study.

The *mPRDX4*$^{-/y}$ mice were previously generated by Fujii and coworkers (2) by cloning and sequencing *mPRDX4* genomic DNA from a b129/SVJ mouse genomic library (Stratagene), and constructing a targeting vector using the cloned DNA fragment. As the chimeric male mice generated from the embryonic stem cells were infertile, Fujii and coworkers performed intracytosolic sperm injection into blastocysts and implanted them into the uteri of pseudopregnant C57BL/6 female mice (2).

Blood pressure

Blood pressure was measured in conscious mice using the tail-cuff method (Model MK-2000; Muromachi Kikai Co., Ltd.), as previously described (1).

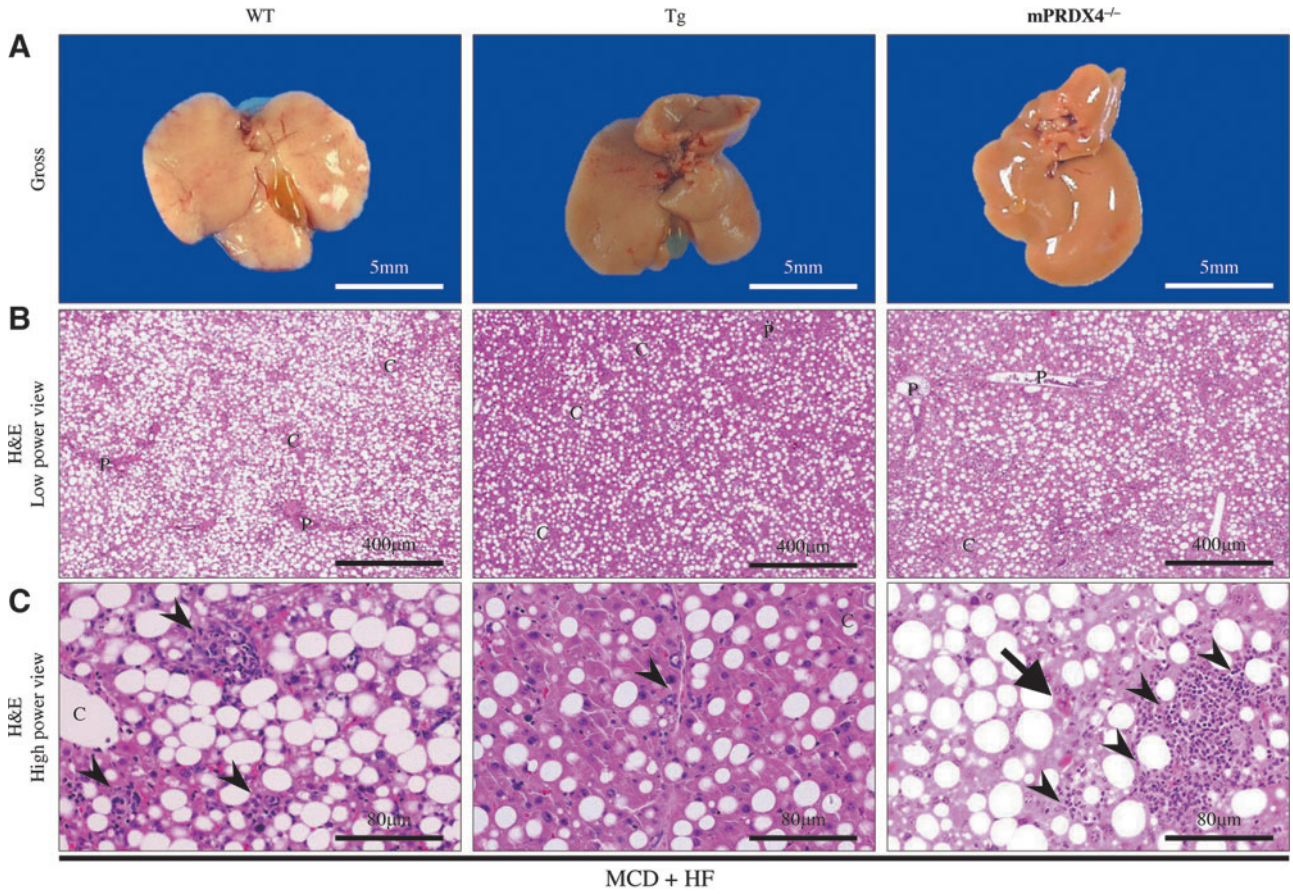

D

MCD + HF	WT	Tg	mPRDX4$^{-/-}$
Steatosis score	2.80 ± 0.20	2.20 ± 0.20*	2.60 ± 0.24
Inflammation score	2.20 ± 0.20	1.40 ± 0.24*	2.80 ± 0.20*
NASH score	5.00 ± 0.32	3.60 ± 0.24*	5.40 ± 0.24

SUPPLEMENTARY FIG. S3. Histological and morphological analyses in livers of mice fed the methionine- and choline-deficient high-fat (MCD+HF) diet. (A) Gross appearance of the livers from mice fed MCD+HF diet for 4 weeks (MCD+HF, $n=5$ mice per group). The livers from WT mice were pale and yellow in color, whereas livers from Tg mice showed mild yellow discoloration. The livers of *mPRDX4*$^{-/y}$ mice showed almost similar to those from WT mice. Scale bar = 5 mm. **(B)** Hematoxylin and eosin (H&E) staining revealed markedly lipid accumulation and inflammation in mice fed the MCD+HF diet for 4 weeks (MCD+HF, $n=5$ mice per group). The livers from Tg mice contained moderate hepatocyte lipid deposition with scant inflammatory foci. By contrast, the livers from WT mice contained significantly more lipid droplets. The livers from *mPRDX4*$^{-/y}$ mice also exhibited progressive steatosis almost similar to those from WT mice. C, central vein; P, portal vein. Original magnification: ×40, scale bar = 400 μm. **(C)** High-power view of H&E-stained sections revealed macrovesicular and microvesicular steatosis throughout the entire lobules in the livers from WT and *mPRDX4*$^{-/y}$ mice, and these regions coexisted with lobular and perivenular inflammation (*arrowheads*) (MCD+HF, $n=5$ mice per group). Foci of spotty hepatocyte necrosis were occasionally seen particularly in the livers from *mPRDX4*$^{-/y}$ mice (*arrow*). By contrast, the livers from Tg mice showed very mild steatosis and inflammation. C, central vein. Original magnification: ×200, scale bar = 80 μm. **(D)** Scoring fat accumulation and inflammation in the nonalcoholic steatohepatitis (NASH) livers from mice fed the MCD+HF diet for 4 weeks (MCD+HF, $n=5$ mice per group). Hepatic steatosis and inflammation scores were significantly greater in WT and *mPRDX4*$^{-/y}$ mice than in Tg mice. Additionally, the hepatic inflammation score in *mPRDX4*$^{-/y}$ mice was significantly more progressive than in WT mice, although the difference of hepatic steatosis scores was not significant. Consequently, NASH scores were significantly greater in WT and *mPRDX4*$^{-/y}$ mice than in Tg mice. Values are means ± SE. *$p < 0.05$.

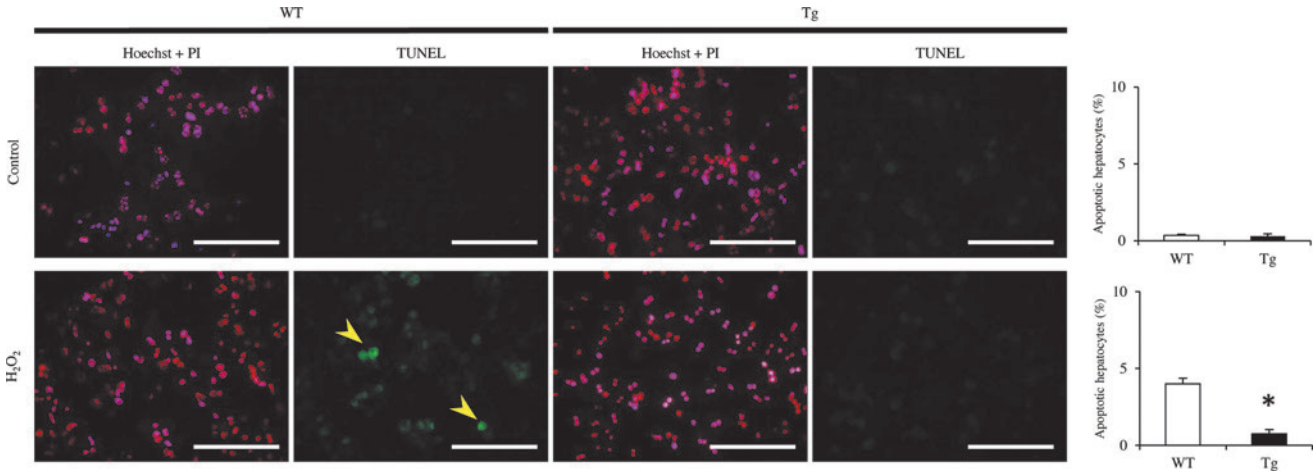

SUPPLEMENTARY FIG. S4. Analysis of oxidative stress-induced apoptosis in hepatocytes harvested from WT and Tg mice. Cultured hepatocytes were analyzed by fluorescence double staining with propidium iodide (PI; red-orange) and Hoechst 33258 (blue); terminal deoxynucleotidyl transferase end-labeling (TUNEL)-positive apoptotic hepatocytes were also analyzed in the same fields (green). Hepatocytes from WT or Tg mice were incubated with a medium alone (control) or in a medium containing 100 μM H_2O_2. Although only a very small number of apoptotic cells were observed in the untreated control hepatocytes, the percentage of TUNEL-positive hepatocytes was significantly higher in cells from WT mice (*arrowheads*) than in those from Tg mice after oxidative stress stimulation. Apoptotic cell counts for 3–6 representative fields ($\sim$100 cells) are shown for each condition, and are expressed as the percentage of total cells stained with TUNEL or PI. Values are means ± SE of at least three separate experiments ($n = 3$ per condition). Original magnification: ×200, scale bar = 200 μm. *$p < 0.05$.

Preparation of liver hepatocytes

Liver hepatocytes were isolated from 8-week-old male Tg and WT mice fed a normal chow diet. All mice were anesthetized by intraperitoneal injection with a pentobarbital solution. The abdominal cavity was opened, and the mesenteric and bilateral renal arteries were ligated. A ligature was placed around the portal vein at a site distal to the bifurcation and another around the inferior vena cava at a site proximal to the mesenteric artery. A tapered polyethylene cannula connected to a perfusion apparatus was inserted into the portal vein and was ligated in place. An 18G needle was also inserted into the vena cava and ligated in place. Then, a liver perfusion medium (GIBCO17701-038; Gibco) and a collagenase type II solution medium (Gibco), mixed with the oxygen and carbon dioxide mixture (95:5) at 37°C, were injected into the cannula (4.5 ml/min). The collected cells were washed with the Dulbecco's modified Eagle's medium (DMEM), cultured in the

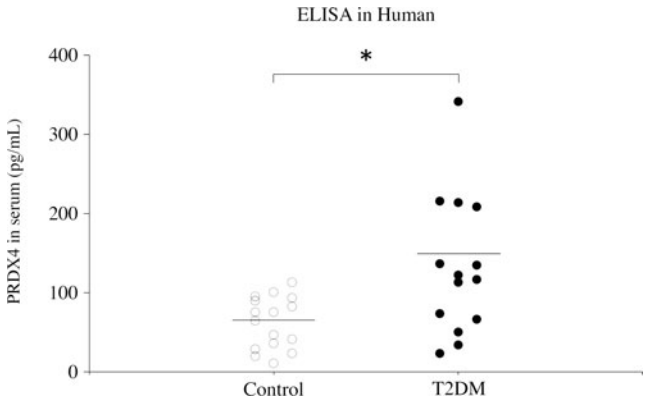

SUPPLEMENTARY FIG. S5. Serum hPRDX4 protein levels in patients with type 2 diabetes mellitus (T2DM) and in healthy adults. Results of enzyme-linked immunosorbent assays showed that serum hPRDX4 levels were significantly higher in patients with T2DM than in healthy adults as a control group ($n = 15$ per group). Values are means ± SE. *$p < 0.05$.

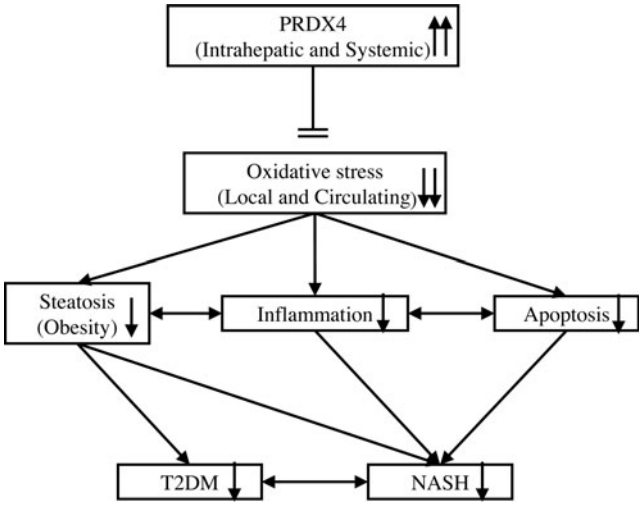

SUPPLEMENTARY FIG. S6. Summary of roles of PRDX4 in T2DM and NASH. This diagram depicts the possible roles of PRDX4 in the nongenetic mouse model of T2DM and NASH.2

SUPPLEMENTARY TABLE S1. RT-PCR AND REAL-TIME RT-PCR PRIMERS

Gene	Forward primer	Reverse primer	Taqman probe
real-time PCR primer			
Bax	ATGGCTGGACACTGGACTTC	GAGGACTCCAGCCACAAAGATG	TGGCTGGGAAGGCCTCCTCTCCTACT
Caspase-3	AAGCCGAAACTCTTCATCATTCAG	AGCCTCCACCGGTATCTTCTG	TGGACTGTGGCATTGAGACAGACAGTGG
mPRDX1	TGTGGATTCTCACTTCTGTCATCTG	GTGCGCTTGGGATCTGATATTAAG	CACACCCAAGAAACAAGGAGGATTGGGA
mPRDX2	CCCAGAATTACGGCGTGTTG	CCCTTGGCATCGATGATAAAGA	AATGATGAGGGCATTGCTTACAGGG
mPRDX3	GGTGCTTTTCTTCTACCCTTTGG	CACAGTTTACATCATCATGAAATTCATTGG	TTGTGTGTCCTACAGAAATTGTTGC
mPRDX4	TGGACGAGACACTGCGTTTG	CTGGATCTGGGATTATTGTTTCACTAC	ACACTGACAAGCATGGAGAAGTCTGCCC
mPRDX5	GGAAGGCGACAGACTTATTATTGG	CTCCACGTTCAGTGCCTTCAC	CGTCGGCTGAAAAGGTTCTCCATGGT
mPRDX6	GCCAAGAGGAATGTTAAGTTGATTG	GTTTCACCATTGTAAGCATTGATGTC	CAATAGACAGTGTTGAGGATCATCATCTTGCCTGG
hPRDX4	GTTGATTCACAGTTTACCCATTTGG	TCTGATGGGTCAAATCTGAAAGAAG	CTCGAAGACAAGGAGGACTTGGGCCA
TNF-α	CCCAGACCCTCACACTCAGATC	TGCTCCTCCACTTGGTGGTT	ATTCGAGTGACAAGCCTGTAGCCCACG
TNFR2	TGGTCTGATTGTTGGAGTGACATC	GGATTTCTCATCAGGCACATGAG	TGCATCATCCTGGTGCAGAGGAAAAAGA
AdipoR1	CATGGCCACAGACCACCTATG	CAAATAGCACAAAACCAAGCAGATG	TCAAGAGCATCTTCCGCATCCACACAG
AdipoR2	GGTCTCCCGACTCTTCTCTAAATTG	TTGTGGGTTACAGTAGAAAGAATAATAAAGC	CTGGTATTGCTCTTCTGATCATGGGAAGTTTTGT
18s rRNA TaqMan Ribosomal RNA Control Reagents VIC Probe (Applied Biosystems, Cat. No. 4308329)			
RT-PCR primer			
mPRDX4	AAGATCTCCAAGCCAGCACC	ATGCTTGTCAGTGTACTGGAAGG	
hPRDX4	ATGGAGGCGCTGCCGCTGCTAGC	GTTCCTTCCCAGTAGGGCGCTGG	

DMEM supplemented with 10% fetal bovine serum, 1% penicillin–streptomycin (Gibco), and 2 mM glutamine (Gibco) at a density $2–3\times10^5$ cells/cm^2, and placed onto six-well glass slides in an incubator for >3 days. Adherent cells (hepatocytes) were maintained in the medium.

For hPRDX4 staining, the hepatocytes were fixed in 95% acetone for 30 s at room temperature and permeabilized in 0.1% Triton X-100 for 2 min at 4°C. Cells were then stained with a rabbit anti-hPRDX4 polyclonal antibody (1:100; Affinity BioReagents) for 1 h, washed with phosphate-buffered saline, and reacted with fluorescein isothiocyanate-conjugated anti-rabbit IgG (Invitrogen, Life Technologies Japan Ltd.) for fluorescence staining. The isolated hepatocytes were observed and immediately photographed with a Nikon ECLIPSE E600 inverted fluorescence microscope (Nikon), as previously described (1).

To confirm that the hPRDX4 protein was localized to the endoplasmic reticulum (ER), we performed immunofluorescence microscopy. Briefly, hepatocytes obtained from Tg mice were incubated at 37°C for 1 h in ER-Tracker™ Blue-White DPX (E-12353; Molecular Probes Life Technologies) before fixation in 3.7% formaldehyde, followed by rabbit anti-hPRDX4 polyclonal antibody staining (Affinity BioReagents) (1).

Analysis of oxidative stress-induced apoptosis in hepatocytes

Adherent hepatocytes were plated onto six-well glass slides for terminal deoxynucleotidyl transferase end-labeling (TUNEL) assays. The hepatocytes from Tg and WT mice were incubated for 17 h in a medium alone as a control, or in a medium containing 100 μM H_2O_2, as previously described (1, 5). The hepatocytes were then fixed in 95% acetone for 30 s at room temperature and permeabilized in 0.1% Triton X-100 for 2 min at 4°C. Hepatocytes were then stained with the TUNEL reaction mixture (Roche Applied Science) for 30 min at room temperature and incubated with Hoechst 33258 (0.5 μg/ml; Dojindo) and propidium iodide (PI; 5 μg/ml; Sigma) for fluorescence double staining. Cells were then observed and immediately photographed with a Nikon ECLIPSE E600 inverted fluorescence microscope. The number of TUNEL-positive (green) cells, PI-positive (red-orange) cells, and total cells were counted in three to six representative fields (~100 cells/field). The number of apoptotic hepatocytes was expressed as a percentage of the total number of cells. We performed more than three independent experiments.

hPRDX4 ELISA in T2DM human patients

The circulation level of hPRDX4 derived from peripheral blood cells, was measured in sera from patients with T2DM or healthy adult volunteers (as a control group), using commercial enzyme-linked immunosorbent assays (hPRDX4; Abnova). The patients and healthy individuals were matched for sex (100% male) and age (control: 53.3 ± 3.8 years, range 24–72 years *vs*. T2DM: 54.4 ± 3.6 years, range 33–78 years). We excluded people with any of the following: an evidence of current infective, inflammatory, or neoplastic conditions; hepatic or renal severe dysfunction; and participation in a drug trial within the previous 30 days. T2DM was diagnosed using the criteria of the American Diabetes Association (4). The mean duration of T2DM was 8 years, and ranged 1.5–30.0

years. The Ethics Committee of Experimentation, University of Occupational and Environmental Health (Kitakyushu, Japan) approved all the procedures in humans (permission no. H24–140), and all participants gave written informed consent.

Statistical analysis

Results are expressed as means ± standard error. Significant differences were analyzed using the Student's *t*-test, the Welch's *t*-test, or one-way analysis of variance (ANOVA), where appropriate. In all cases when ANOVA methodology was employed, the Tukey's multiple comparison *post hoc* test was used. Values of $p < 0.05$ were considered to be statistically significant.

Supplementary References

1. Guo X, Yamada S, Tanimoto A, Ding Y, Wang KY, Shimajiri S, Murata Y, Kimura S, Tasaki T, Nabeshima A, Watanabe T, Kohno K, and Sasaguri Y. Overexpression of peroxiredoxin 4 attenuates atherosclerosis in apolipoprotein E knockout mice. *Antioxid Redox Signal* 17: 1362–1375, 2012.
2. Iuchi Y, Okada F, Tsunoda S, Kibe N, Shirasawa N, Ikawa M, Okabe M, Ikeda Y, and Fujii J. Peroxiredoxin 4 knockout results in elevated spermatogenic cell death via oxidative stress. *Biochem J* 419: 149–158, 2009.
3. Meier JL and Stinski MF. Regulation of human cytomegalovirus immediate-early gene expression. *Intervirology* 39: 331–342, 1996.
4. The Expert Committee on the Diagnosis and Classification of Diabetes Mellitus. Report of the Expert Committee on the Diagnosis and Classification of Diabetes Mellitus. *Diabetes Care* 20: 1183–1197, 1997.
5. Watanabe T, Otsu K, Takeda T, Yamaguchi O, Hikoso S, Kashiwase K, Higuchi Y, Taniike M, Nakai A, Matsumura Y, Nishida K, Ichijo H, and Hori M. Apoptosis signal-regulating kinase 1 is involved not only in apoptosis but also in non-apoptotic cardiomyocyte death. *Biochem Biophys Res Commun* 333: 562–567, 2005.
6. Yamada S, Ding Y, and Sasaguri Y. Peroxiredoxin 4: critical roles in inflammatory diseases. *J UOEH* 34: 27–39, 2012.